Computing Rational Border Curves of Melanoma and Other Skin Lesions from Medical Images with Bat Algorithm

Akemi Gálvez
Toho University
Funabashi, Japan
University of Cantabria
Santander, Spain
galveza@unican.es

Iztok Fister Jr.
University of Maribor
Maribor, Slovenia
iztok.fister1@um.si

Eneko Osaba
TECNALIA
Derio, Spain
eneko.osaba@tecnalia.com

Iztok Fister
University of Maribor
Maribor, Slovenia
iztok.fister@um.si

Javier Del Ser
University of the Basque Country
Bilbao, Spain
TECNALIA
Derio, Spain
javier.delser@tecnalia.com

Andrés Iglesias*
Toho University
Funabashi, Japan
University of Cantabria
Santander, Spain
iglesias@unican.es

ABSTRACT

Border detection of melanoma and other skin lesions from images is an important step in the medical image processing pipeline. Although this task is typically carried out manually by the dermatologists, some recent papers have applied evolutionary computation techniques to automate this process. However, these works are only focused on the polynomial case, ignoring the more powerful (but also more difficult) case of rational curves. In this paper, we address this problem with rational Bézier curves by applying the bat algorithm, a popular bio-inspired swarm intelligence technique for optimization. Experimental results on two examples of medical images of melanomas show that this method is promising, as it outperforms the polynomial approach and can be applied to medical images without further pre/post-processing.

KEYWORDS

Healthcare, swarm intelligence, bio-inspired optimization, bat algorithm, rational curves, image segmentation, border detection, medical images, melanoma, skin lesions

ACM Reference Format:
Akemi Gálvez, Iztok Fister Jr., Eneko Osaba, Iztok Fister, Javier Del Ser, and Andrés Iglesias. 2019. Computing Rational Border Curves of Melanoma and Other Skin Lesions from Medical Images with Bat Algorithm. In *Proceedings of the Genetic and Evolutionary Computation Conference 2019 (GECCO '19).* ACM, New York, NY, USA, 8 pages. https://doi.org/10.1145/nnnnnnn.nnnnnnn

* Corresponding author

GECCO '19, July 13–17, 2019, Prague, Czech Republic

ACM ISBN 978-x-xxxx-xxxx-x/YY/MM. . . $15.00
https://doi.org/10.1145/nnnnnnn.nnnnnnn

1 INTRODUCTION

1.1 Motivation

Cancer is one of the most critical and important concerns of public and private medical and healthcare systems worldwide. Some simple figures to put the problem into a proper perspective: one in 5 men and one in 6 women worldwide will develop cancer during their lifetime, and one in 8 men and one in 11 women will die from the disease. It has also been reported that more than 90 million people has been affected by cancer in 2015, with more than 15 million cases arising every year. The effects of cancer are devastating, with more than 9 million deaths annually and medical costs of more than 1.3 trillion USD in 2015. According to a recent report from the International Agency for Research Cancer of the World Health Organization[1], these figures are still raising consistently, with 18.1 million new cases and 9.6 million deaths in 2018.

This increasing cancer burden is due to several factors, including population growth and ageing as well as the changing prevalence of certain causes of cancer related to economic development and new social customs. For instance, the popularity of sunlight exposure is linked to a dramatic increase in the number of cases of skin cancer and other skin diseases. According to a report from the Australian Cancer Council[2]: *"Almost all skin cancers (approximately 99% of non-melanoma skin cancers and 95% of melanoma) are caused by too much UV radiation from the sun or other sources such as solaria (solariums, sunbeds, and sun lamps)."*

As a matter of fact, the number of cases of skin cancer and other skin diseases is dramatically increasing in recent years. As a consequence, healthcare systems are increasingly demanded for diligent and accurate diagnosis and treatment of skin lesions. Time is a key factor in this process, since early detection is critical for an efficient treatment of melanoma and other malignant skin lesions. It has been widely reported

[1] Web site: www.who.int/cancer
[2] Web site: www.cancercouncil.com.au

that the five-year survival rate is about 99% for stage 0 melanoma (in situ), when the tumor is confined to the epidermis, while it is only 7% $\sim$ 20% for stage 4 melanoma, when the cancer has spread to other parts of the body. These figures are a clear evidence of the important role of prompt detection and accurate diagnosis.

The most common diagnostic procedure for skin lesions is the visual inspection by a specialist. However, several types of skin cancer such as melanoma are difficult to discriminate visually from other skin lesions. Other diagnosis procedures include the popular ABCDE method, the Menzies scale, the 7-point checklist, and different types of biopsy [10, 24]. Unfortunately, these procedures rely strongly on the clinical experience of the specialists. Consequently, the diagnostic procedures are time-consuming and the results are prone to errors, due to the difficulty and subjectivity of human diagnosis. Other kind of procedures involve imaging tests, including X-ray, computer tomography (CT) scan, magnetic resonance imaging (MRI) scan, positron emission tomography (PET) scan and others. In most cases, these procedures are used to track the possible spread of melanoma to other parts of the body rather than for early identification. Also, there is still some subjectivity related to the visual perception of images. This makes the use of advanced computer-aided image processing techniques a very useful tool as a second independent diagnosis to improve the decision-making procedures and workflow by clinicians, and for many other purposes. As a result, the computerized analysis of medical images is becoming a very active area of research in the biomedical and healthcare fields.

A major goal in computer-aided medical image processing for dermatology is to develop reliable computer tools for accurate identification and classification of melanoma and other skin lesions. This is also the motivation of this work. Obviously, this is a herculean task that cannot be addressed in a single paper. In this work, we will restrict ourselves to a particular task of the full image processing pipeline, namely, the computation of the border curves of melanoma and other skin lesions from medical images for image segmentation. We refer the interested readers to [20, 25] for two interesting and comprehensive reviews on techniques and algorithms for general computer-aided diagnosis of skin lesions.

1.2 Computer-aided methods for medical image processing in dermatology

Two commonly used image acquisition methods for early diagnosis of skin lesions are macroscopic images and dermoscopy. The former consists of taking a close picture of the skin lesion with a standard digital camera and send it to the specialist for remote examination. This option is of great help for patients with difficult access to a dermatologist, such as those living in remote areas or handicapped people. Dermoscopy is more precise and reduces screening errors as it enhances discrimination between real melanoma and other skin lesions [1, 4]. Of course, both methods depend on the human factor for accurate diagnosis. Although removing the human factor in diagnostic procedures entirely is neither convenient nor desirable, it turns out that reliable and accurate automatic methods could arguably help to alleviate the work load on human specialists and reduce diagnostic errors.

The standard approach in automatic medical image processing of skin lesions consists of three stages: 1) image segmentation; 2) feature extraction and feature selection; and 3) lesion classification. Image segmentation aims to identify the area of the skin lesion and separate it from the background. This stage is very important, as it represents the starting point for the whole pipeline and it affects the accuracy of the next stages. Popular segmentation approaches include thresholding methods [5, 15], edge-based methods [2], clustering methods [27, 37], level set methods [23] and active contours [22], among others.

An important task in image segmentation is border detection, which means computing the border between the skin lesion and the surrounding healthy skin area. This border curve is very helpful for diagnosis, because it provides valuable information for several tests (for instance, irregular borders are a good indicator of possible malignant tumors). Usually, the border detection is performed manually by the dermatologists, who select a set of feature points by simple visual inspection. Such feature points are then joined with a polygonal line to enclose the area of the lesion. However, this procedure does not represent the real process accurately, since the border of skin lesions rarely happens to be linear. In addition, interpolation schemes enforce the border to pass through *all* feature points, even if they are simple outliers due to measurement noise or other problems. Approximation schemes, in which the curve passes *near* the feature points, are more advantageous in terms of accuracy, computer memory, and data storage capacity, as the border can be accurately described by a few tens of parameters even for large collections of feature points. This is the problem addressed in this paper, as explained in detail in next section.

2 THE PROBLEM

The problem to be solved in this paper can be formulated as follows: suppose that we are provided with a sorted collection of feature points $\{\boldsymbol{\Delta}_i\}_{i=1,\ldots,\kappa}$ in $\mathbb{R}^2$ obtained from medical images by a trained dermatologist. Such feature points correspond to the boundary curve between a skin lesion or tumor and the skin background. Note that in this paper vectors are denoted in bold. Since the feature points are collected in a manual way, they are subjected to measurement noise, irregular sampling, and other artifacts. Therefore, an approximation scheme based on a smooth mathematical curve is generally more suitable for border detection than the linear interpolation given by a polyline connecting the feature points through simple straight lines. Consequently, our goal is to compute a parametric curve $\boldsymbol{\Phi}(\tau)$ performing discrete approximation of the feature points $\{\boldsymbol{\Delta}_i\}_i$ in the least-squares sense.

Several families of approximation functions can be used for this task. Among them, the free-form parametric curves

(such as Bézier and B-spline curves) are popular choices, because of their flexibility and wide applicability in academia and industrial settings [6, 26]. Some previous papers have addressed the case of Bézier curves using different swarm intelligence methods, such as the bat algorithm [11] and the cuckoo search algorithm [12]. A very recent paper applies a hybrid modified firefly algorithm to this problem [13]. However, in all these cases, only the polynomial case has been considered, while surprisingly the (more powerful) rational case has been ignored so far. This paper aims at filling this gap. In line with this, in this work we focus on the particular case of rational Bézier curves [8, 26].

Mathematically, a *free-form rational Bézier curve* $\mathbf{\Phi}(\tau)$ *of degree* η is defined as:

$$\mathbf{\Phi}(\tau) = \frac{\sum_{j=0}^{\eta} \omega_j \mathbf{\Lambda}_j \phi_j^{\eta}(\tau)}{\sum_{j=0}^{\eta} \omega_j \phi_j^{\eta}(\tau)} \tag{1}$$

where $\mathbf{\Lambda}_j$ are vector coefficients called the *poles*, ω_j are their scalar weights, $\phi_j^{\eta}(\tau)$ are the *Bernstein polynomials of index* j *and degree* η, given by:

$$\phi_j^{\eta}(\tau) = \binom{\eta}{j} \tau^j \ (1-\tau)^{\eta - j}$$

with $\binom{\eta}{j} = \frac{\eta!}{j!(\eta - j)!}$, and τ is the *curve parameter*, defined on the finite interval $[0, 1]$. By convention, $0! = 1$.

Now, our optimization problem consists of computing all parameters (i.e. poles $\mathbf{\Lambda}_j$, weights ω_j, and parameters τ_i associated with the $\mathbf{\Delta}_i$, for $i = 1, \ldots, \kappa$, $j = 0, \ldots, \eta$) of the rational Bézier curve $\mathbf{\Phi}(\tau)$ approximating the feature points better in the least-squares sense. This means minimizing the least-squares error, Υ, defined as the sum of squares of the residuals:

$$\Upsilon = \underset{\substack{\{\tau_i\}_i \\ \{\mathbf{\Lambda}_j\}_j \\ \{\omega_j\}_j}}{\text{minimize}} \left[\sum_{i=1}^{\kappa} \left(\mathbf{\Delta}_i - \frac{\sum_{j=0}^{\eta} \omega_j \mathbf{\Lambda}_j \phi_j^{\eta}(\tau_i)}{\sum_{j=0}^{\eta} \omega_j \phi_j^{\eta}(\tau_i)} \right)^2 \right]. \tag{2}$$

Now, taking:

$$\varphi_j^{\eta}(\tau) = \frac{\omega_j \phi_j^{\eta}(\tau)}{\sum_{k=0}^{\eta} \omega_k \phi_k^{\eta}(\tau)} \tag{3}$$

Eq. (2) becomes:

$$\Upsilon = \underset{\substack{\{\tau_i\}_i \\ \{\mathbf{\Lambda}_j\}_j \\ \{\omega_j\}_j}}{\text{minimize}} \left[\sum_{i=1}^{\kappa} \left(\mathbf{\Delta}_i - \sum_{j=0}^{\eta} \mathbf{\Lambda}_j \varphi_j^{\eta}(\tau) \right)^2 \right], \tag{4}$$

which can be rewritten in matrix form as:

$$\mathbf{\Omega}.\mathbf{\Lambda} = \mathbf{\Xi} \tag{5}$$

called the *normal equation*, where:

$$\mathbf{\Omega} = [\Omega_{i,j}] = \left[\left(\sum_{k=1}^{\kappa} \varphi_i^{\eta}(\tau_k) \varphi_j^{\eta}(\tau_k) \right)_{i,j} \right],$$

$$\mathbf{\Xi} = [\Xi_j] = \left[\left(\sum_{k=1}^{\kappa} \mathbf{\Delta}_k \varphi_j^{\eta}(\tau_k) \right)_{j} \right],$$

$\mathbf{\Lambda} = (\mathbf{\Lambda}_0, \ldots, \mathbf{\Lambda}_\eta)^T$, for $i, j = 0, \ldots, \eta$, and $(.)^T$ means the transposition of a vector or a matrix. In general, $\kappa >> \eta$ meaning that the system (5) is over-determined. If values are assigned to the τ_i, our problem can be solved as a classical linear least-squares minimization, with the coefficients $\{\mathbf{\Lambda}_i\}_{i=0,\ldots,\eta}$ as unknowns. This problem can readily be solved by standard numerical techniques. On the contrary, if the values of τ_i are treated as unknowns, the problem becomes much more difficult. Indeed, since the polynomial blending functions $\phi_j^{\eta}(\tau)$ are nonlinear in τ and so are the rational blending functions $\varphi_j^{\eta}(\tau)$, the least-squares minimization of the errors is a nonlinear continuous optimization problem. Note also that in many practical cases the number of data points can be extremely large, meaning that we have to deal with a large number of unknowns. In other words, we are dealing with a high-dimensional problem. It is also a multimodal problem, since there might be more than one set of parameter values leading to the optimal solution.

To summarize, the interplay among all sets of unknowns (data parameters, poles, and weights) leads to a very difficult over-determined, multimodal, multivariate, continuous, nonlinear optimization problem. In this work, we are interested to solve this general problem. Therefore, instead of making assumptions about the values of the free parameters, we are aimed at computing all of them in an integrated way.

Unfortunately, it has been proved that the classical mathematical optimization methods are not able to solve this difficult problem. As a consequence, there has been a great interest to explore other alternatives, including artificial intelligence techniques. Among them, the evolutionary computation methods of biological inspiration are very powerful tools for continuous optimization [7, 32]. For instance, as discussed above, swarm intelligence methods have already been applied to quite close (but simpler) problems, such as the border detection problem with polynomial curves [11–13]. Encouraged by these positive results, we follow a similar strategy here for this (more difficult) rational problem. In particular, we address our optimization problem by using a powerful bio-inspired method called bat algorithm and described in next section.

3 THE BAT ALGORITHM

The *bat algorithm* is a bio-inspired swarm intelligence algorithm originally proposed by Xin-She Yang in 2010 to solve optimization problems [33–35]. The algorithm is based on the echolocation behavior of bats. The author focused particularly on microbats, as they use a type of sonar called

Require: (Initial Parameters)
Population size: $\mathcal{P}$
Maximum number of generations: $\mathcal{G}_{max}$
Loudness: $\mathcal{A}$
Pulse rate: r
Maximum frequency: f_{max}
Dimension of the problem: d
Objective function: $\phi(\mathbf{x})$, with $\mathbf{x} = (x_1, \ldots, x_d)^T$
Random number: $\theta \in U(0,1)$
1: $g \leftarrow 0$
2: Initialize the bat population $\mathbf{x}_i$ and $\mathbf{v}_i$, $(i = 1, \ldots, n)$
3: Define pulse frequency f_i at $\mathbf{x}_i$
4: Initialize pulse rates r_i and loudness $\mathcal{A}_i$
5: **while** $g < \mathcal{G}_{max}$ **do**
6: **for** $i = 1$ **to** $\mathcal{P}$ **do**
7: Generate new solutions by adjusting frequency,
8: and updating velocities and locations //eqns. (6)-(8)
9: **if** $\theta > r_i$ **then**
10: $\mathbf{s}^{best} \leftarrow \mathbf{s}^g$ //select the best current solution
11: $\mathbf{ls}^{best} \leftarrow \mathbf{ls}^g$ //generate a local solution around $\mathbf{s}^{best}$
12: **end if**
13: Generate a new solution by local random walk
14: **if** $\theta < \mathcal{A}_i$ *and* $\phi(\mathbf{x_i}) < \phi(\mathbf{x}^*)$ **then**
15: Accept new solutions
16: Increase r_i and decrease $\mathcal{A}_i$
17: **end if**
18: **end for**
19: $g \leftarrow g + 1$
20: **end while**
21: Rank the bats and find current best $\mathbf{x}^*$
22: **return** $\mathbf{x}^*$

Algorithm 1: Bat algorithm pseudocode

echolocation, with varying pulse rates of emission and loudness, to detect prey, avoid obstacles, and locate their roosting crevices in the dark.

3.1 Basic rules

The idealization of the echolocation of microbats can be summarized as follows (see [33] for details):

(1) Bats use echolocation to sense distance and distinguish between food, prey and background barriers.
(2) Each virtual bat flies randomly with a velocity $\mathbf{v}_i$ at position (solution) $\mathbf{x}_i$ with a fixed frequency f_{min}, varying wavelength λ and loudness A_0 to search for prey. As it searches and finds its prey, it changes wavelength (or frequency) of their emitted pulses and adjust the rate of pulse emission r, depending on the proximity of the target.
(3) It is assumed that the loudness will vary from an (initially large and positive) value A_0 to a minimum constant value A_{min}.

In order to apply the bat algorithm for optimization problems more efficiently, some additional assumptions are strongly advisable. In general, we assume that the frequency f evolves on a bounded interval $[f_{min}, f_{max}]$. This means that the wavelength λ is also bounded, because f and λ are related to each other by the fact that the product $\lambda.f$ is constant. For practical reasons, it is also convenient that the largest wavelength is chosen such that it is comparable to the size of the domain of interest (the search space, for optimization problems). For simplicity, we can assume that $f_{min} = 0$, so $f \in [0, f_{max}]$. The rate of pulse can simply be in the range $r \in [0, 1]$, where 0 means no pulses at all, and 1 means the maximum rate of pulse emission.

3.2 The algorithm

With these idealized rules indicated above, the basic pseudocode of the bat algorithm is shown in Algorithm 1. Basically, the algorithm considers an initial population of $\mathcal{P}$ individuals (bats). Each bat, representing a potential solution of the optimization problem, has a location $\mathbf{x}_i$ and velocity $\mathbf{v}_i$. The algorithm initializes these variables (lines 1-2) with random values within the search space. Then, the pulse frequency, pulse rate, and loudness are computed for each individual bat (lines 3-4). Then, the swarm evolves in a discrete way over generations (line 5), like time instances (line 19) until the maximum number of generations, $\mathcal{G}_{max}$, is reached (line 20). For each generation g and each bat (line 6), new frequency, location and velocity are computed (lines 7-8) according to the following evolution equations:

$$f_i^g = f_{min}^g + \beta(f_{max}^g - f_{min}^g) \quad (6)$$

$$\mathbf{v}_i^g = \mathbf{v}_i^{g-1} + [\mathbf{x}_i^{g-1} - \mathbf{x}^*]\, f_i^g \quad (7)$$

$$\mathbf{x}_i^g = \mathbf{x}_i^{g-1} + \mathbf{v}_i^g \quad (8)$$

where $\beta \in [0, 1]$ follows the random uniform distribution, and $\mathbf{x}^*$ represents the current global best location (solution), which is obtained through evaluation of the objective function at all bats and ranking of their fitness values. The superscript $(.)^g$ is used to denote the current generation g.

The best current solution and a local solution around it are probabilistically selected according to some given criteria (lines 8-11). Then, search is intensified by a local random walk (line 12). For this local search, once a solution is selected among the current best solutions, it is perturbed locally through a random walk of the form:

$$\mathbf{x}_{new} = \mathbf{x}_{old} + \epsilon \mathcal{A}^g \quad (9)$$

where ϵ is a random number with uniform distribution on the interval $[-1, 1]$ and $\mathcal{A}^g =< \mathcal{A}_i^g >$, is the average loudness of all the bats at generation g.

If the new solution achieved is better than the previous best one, it is probabilistically accepted depending on the value of the loudness. In that case, the algorithm increases the pulse rate and decreases the loudness (lines 13-16). This process is repeated for the given number of generations. In general, the loudness decreases once a bat finds its prey (in our analogy, once a new best solution is found), while the rate of pulse emission decreases. For simplicity, the following

values are commonly used: $\mathcal{A}_0 = 1$ and $\mathcal{A}_{min} = 0$, assuming that this latter value means that a bat has found the prey and temporarily stop emitting any sound. The evolution rules for loudness and pulse rate are as follows:

$$\mathcal{A}_i^{g+1} = \alpha \mathcal{A}_i^g \quad (10)$$

$$r_i^{g+1} = r_i^0[1 - exp(-\gamma g)] \quad (11)$$

where α and γ are constants. Note that for any $0 < \alpha < 1$ an any $\gamma > 0$ we have:

$$\mathcal{A}_i^g \to 0, \quad r_i^g \to r_i^0, \quad \text{as } g \to \infty \quad (12)$$

In general, each bat should have different values for loudness and pulse emission rate, which can be computationally achieved by randomization. To this aim, we can take an initial loudness $\mathcal{A}_i^0 \in (0, 2)$ while the initial emission rate r_i^0 can be any value in the interval $[0, 1]$. Loudness and emission rates will be updated only if the new solutions are improved, an indication that the bats are moving towards the optimal solution. As a result, the bat algorithm applies a parameter tuning technique to control the dynamic behavior of a swarm of bats. Similarly, the balance between exploration and exploitation can be controlled by tuning algorithm-dependent parameters.

Bat algorithm is a very promising method that has already been successfully applied to several problems, such as multilevel image thresholding [3], economic dispatch [21], curve and surface reconstruction [16, 17] optimal design of structures in civil engineering [19], robotics [28–31], fuel arrangement optimization [18], planning of sport training sessions [9], fractal image reconstruction [14], and many others. The interested reader is also referred to the general paper in [36] for a comprehensive review of the bat algorithm, its variants and other interesting applications.

4 PROPOSED METHODOLOGY

4.1 Our Method

Our method consists of applying the bat algorithm described in previous section to the border detection problem described in Sect. 2. Solving this optimization problem requires to define some important issues. Firstly, we need an adequate representation of the problem. Each bat, representing a potential solution, corresponds to a vector of the form: $\mathcal{S}_i^g = \{\mathcal{P}_i^g, \mathcal{W}_i^g\}, (i = 1, \ldots, N_{\mathcal{P}})$ with $\mathcal{P}_i^g = \{\tau_{i,1}^g, \ldots, \tau_{i,\kappa}^g\} \in [0, 1]^\kappa$, where the $\{\tau_{i,j}^g\}_{j=1,\ldots,\kappa}$ are strictly increasing parameters, and $\mathcal{W}_i^g = \{\omega_{i,0}^g, \ldots, \omega_{i,\eta}^g\} \in [\omega_{min}, \omega_{max}]^{\eta+1}$, and the superscript g denotes the generation index. The parametric vectors $\mathcal{P}_i^0$, $\mathcal{W}_i^0$ are initialized with random values; then, the elements in $\mathcal{P}_i^0$ are sorted in increasing order. Secondly, we consider the fitness function described by the error functional in (2). We remark however, that this fitting error does not take into account the number of data points. To overcome this drawback, we also compute the $RMSE$ (root-mean squared error), given by:

$$RMSE = \sqrt{\frac{\Upsilon}{\kappa}} \quad (13)$$

Application of our method according to Algorithm 1 yields new bats at each generation, representing the new solutions of our optimization problem. The procedure computes the final values of feature point parameters and weights. Then, inserting them into Eq. (3), we apply least-squares minimization to compute the values of $\{\mathbf{\Lambda}_i\}_{i=0,\ldots,\eta}$ according to Eq. (4). The process is performed iteratively for a given number of iterations $\mathcal{G}_{max}$, until the convergence of the minimization of the error is eventually achieved. The bat with the best global value for our fitness function is taken as the final solution of our problem.

4.2 Parameter Tuning

It is well-known that metaheuristic techniques require proper parameter tuning for good performance [7]. Unfortunately, the choice of suitable parameter values is also strongly problem-dependent. Consequently, our choice is mostly based on empirical results. For the population size we set the value $N_{\mathcal{P}} = 100$, as larger populations take longer without changing our results significantly. The method is executed for $\mathcal{G}_{max}$ iterations. In our simulations, we found that $\mathcal{G}_{max} = 20,000$ is enough to reach convergence for our examples. The initial and minimum loudness, f_{max}, and parameter α are set to 0.5, 0, 2, and 0.6, respectively. We also set the initial pulse rate and parameter γ to 0.5 and 0.4, respectively. However, our results do not change significantly when varying these values slightly. Finally, the parameters ω_{min} and ω_{max} are set to 0.5 and 3, respectively. Unfortunately, a detailed analysis about how all parameters affect the method is not possible here because of limitations of space.

4.3 Implementation Details

Regarding the implementation, our computational work has been performed on a personal PC with a 2.8 GHz Intel Core i7 processor and 16 GB of RAM. The source code has been implemented by the authors in the programming language of the popular numerical program *Matlab*, version 2015b.

5 EXPERIMENTAL RESULTS

5.1 Benchmark and Results

Our method has been applied to several examples of skin lesion images obtained from a digital image archive of the University Medical Center of Groningen, The Netherlands. In this paper we analyze only two of them (labelled as *Example I* and *Example II*) because of limitations of space. They correspond to two medical images of melanomas, displayed in the (top-left) pictures of Figs. 1 and 2, respectively. From the images, a collection of 75 and 127 feature points respectively have been selected by a specialist and joined with a polyline. The medical images along with the feature points connected with the polylines are displayed in the (top-right) pictures of Figs. 1 and 2. We applied our method to these examples by using rational Bézier curves of different degrees, and selecting those minimizing the least-squares functional in Eq. (2). The best fitting rational Bézier curves obtained with our method, corresponding to $\eta = 23$ and $\eta = 32$ respectively,

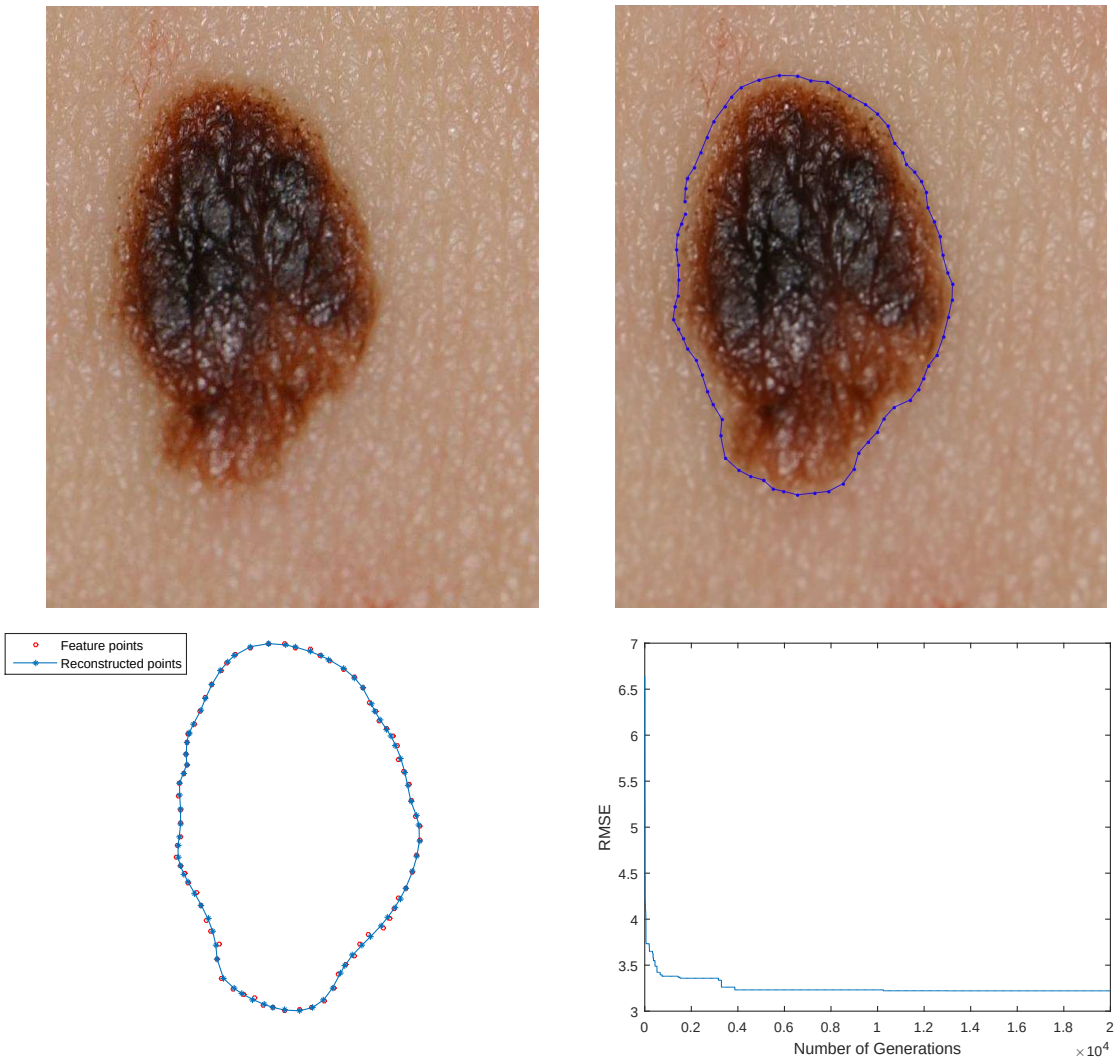

Figure 1: Example I (top-bottom, left-right): original melanoma image; melanoma image and polyline connecting the feature points; original and reconstructed feature points; convergence diagram.

are displayed as blue solid lines in the (bottom-left) pictures of Figs. 1 and 2, respectively. The pictures also display the original and the reconstructed feature points as empty red circles and blue stars, respectively. Finally, the convergence diagram of the RMSE over the generations is shown in the (bottom-right) pictures of both figures.

From the pictures we can see that the method yields a good fitting of the feature points for both examples. This fact is particularly evident in the bottom-left pictures, where the good matching between the original and the reconstructed feature points for both examples is clearly visible. Our visual observations of this good fitting are confirmed by our numerical results, where we obtain an error value of 3.1204 for the first example and 9.3995 for the second one. We also noticed that the approximation is not optimal yet, as expected from an approximation method. In particular, the original data seems to be slightly more oscillating than the reconstructed curve in both cases. We remark, however, that a perfect matching between the original and the reconstructed features points is not actually required for clinical practice.

5.2 Comparative Analysis

It is always convenient to perform a comparative analysis of our method with other approaches described in the literature. Unfortunately, no previous references addressed this problem with rational curves, so our analysis is based on the comparison with the polynomial case with the bat algorithm. Table 1 shows the values of the RMSE obtained with the polynomial approach and our rational approach for the two examples in this paper. For fair comparison, both approaches are addressed with the bat algorithm for the same

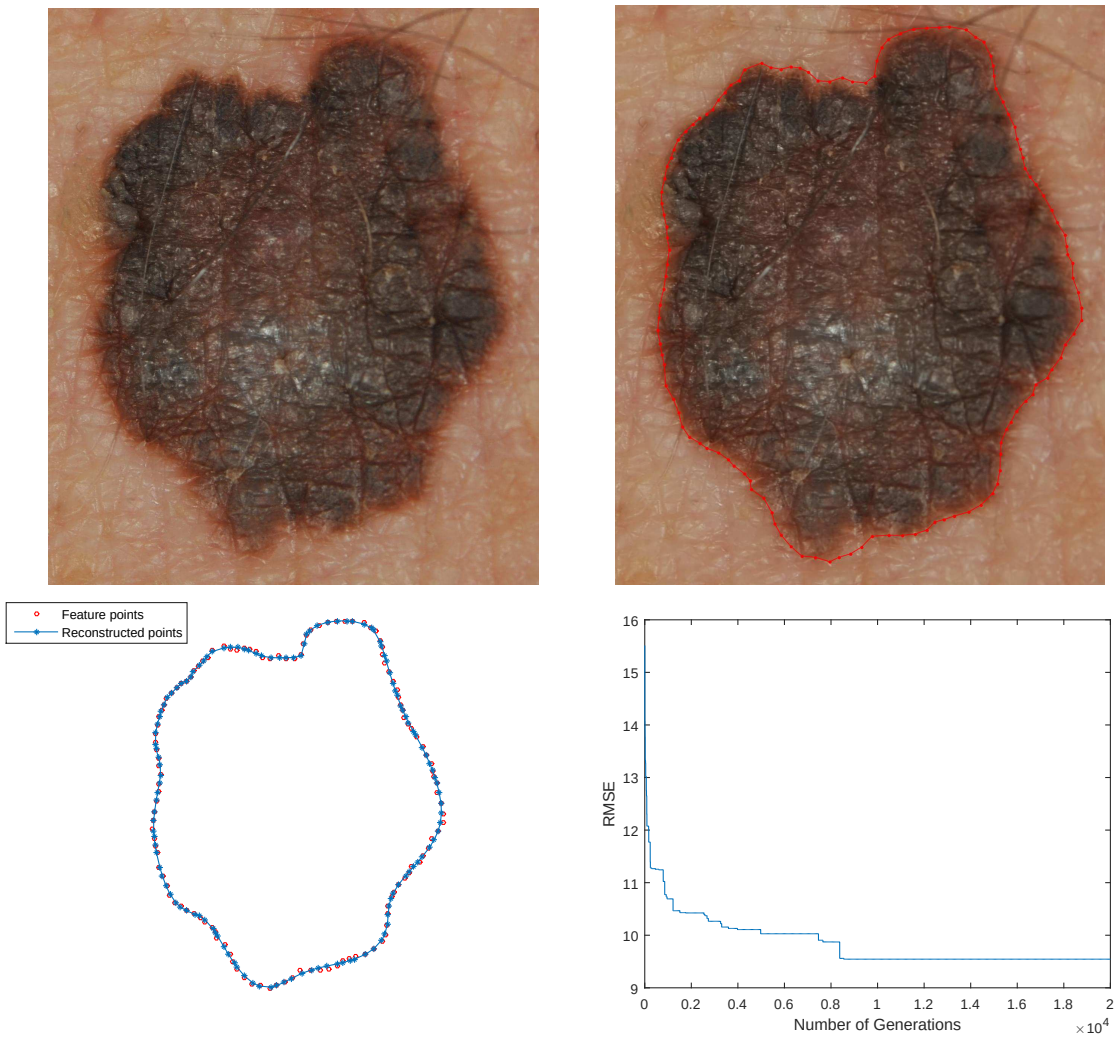

Figure 2: Example II (top-bottom, left-right): original melanoma image; melanoma image and polyline connecting the feature points; original and reconstructed feature points; convergence diagram.

parameter configuration, including the number of iterations and the degree of the curve. As shown in the table, the rational approach outperforms the polynomial one for the two examples in this paper. Although the benchmark used here is too small to draw firm conclusions on a general basis, these results have been validated by other examples from the same digital archive not discussed here because of limitations of space.

Table 1: Comparative results of the polynomial approach and the rational approach (our method) for the two examples in this paper.

	Example I	*Example II*
Polynomial approach:	5.3613	11.7688
Rational approach:	3.1204	9.3995

6 CONCLUSIONS & FUTURE WORK

In this paper, we address the problem of computing the rational border curve of melanomas and other skin lesions from medical images. This is an important task for image segmentation with relevant applications in medical diagnosis of skin diseases. To the best of our knowledge, this is the first work in the field considering rational functions instead of the classical (and much simpler) polynomial functions. Our method is based on the bat algorithm, a popular bio-inspired swarm intelligence technique for optimization. Experimental results on two examples of medical images of melanomas show that the proposed method outperforms the polynomial

approach and can be applied to medical images without further pre/post-processing. We conclude that the method is promising for this problem.

Future work includes expanding our benchmark for a more detailed analysis of our method and carrying out a larger and deeper comparative work including other evolutionary computation methods in the pool of methods for comparison.

ACKNOWLEDGMENTS

A. Galvez and A. Iglesias acknowledge the financial support from the project PDE-GIR of the European Union's Horizon 2020 research and innovation programme under the Marie Sklodowska-Curie grant agreement No 778035, and the project TIN2017-89275-R of the Agencia Estatal de Investigación, Spanish Ministry of Science, Innovation and Universities (Computer Science National Program) and European Funds EFRD (AEI/FEDER, UE). I. Fister Jr. thanks the financial support from the Slovenian Research Agency (Research Core Founding No. P2-0057). E. Osaba and J. Del Ser would like to thank the Basque Government for its funding support through the EMAITEK program. I. Fister acknowledges the financial support from the Slovenian Research Agency (Research Core Founding No. P2-0041).

REFERENCES

[1] Q. Abbas, M. E. Celebi, I. F. Garcia, M. Rashid: Lesion Border Detection in Dermoscopy Images Using Dynamic Programming, Skin Research and Technology, 17(1), 91–100 (2011).

[2] Abbas, A.A., Guo, X., Tan, W.H., Jalab, H.A.: Combined spline and B-spline for an improved automatic skin lesion segmentation in dermoscopic images using optimal color channel. *Journal of Medical Systems*, **38**, 80–80 (2014).

[3] Alihodzic, A., Tuba, M.: Improved bat algorithm applied to multilevel image thresholding. *The Scientific World Journal*, **2014**, article ID 176718, 16 pages (2014).

[4] Argenziano, G., Soyer, H.P., De Giorgi, V.: *Dermoscopy: A Tutorial*. EDRA Medical Publishing & New Media (2002).

[5] M. E. Celebi, H. Iyatomi, H., Schaefer, G., Stoecker, W.V.: Lesion border detection in dermoscopy images. *Computerized Medical Imaging and Graphics*, **33**(2) 148–153 (2009).

[6] Dierckx, P.: *Curve and Surface Fitting with Splines*. Oxford University Press, Oxford (1993)

[7] Engelbrecht, A.P.: *Fundamentals of Computational Swarm Intelligence*. John Wiley and Sons, Chichester, England (2005).

[8] Farin, G.: *Curves and surfaces for CAGD (5th ed.)*. Morgan Kaufmann, San Francisco (2002).

[9] Fister, I., Rauter, S., Yang, X.-S.., Ljubic, K., Fister Jr., I.: Planning the sports training sessions with the bat algorithm. *Neurocomputing*, **149**, Part B, 993–1002 (2015).

[10] Friedman, R.J., Rigel, D.S., Kopf, A.W.: Early detection of malignant melanoma: The role of physician examination and self-examination of the skin. *Cancer Journal for Clinicians*, **35**(3), 130–151 (1985).

[11] Gálvez, A., Fister, I., Fister Jr., I., Osaba, E., Del Ser, J., Iglesias, A.: Automatic fitting of feature points for border detection of skin lesions in medical images with bat algorithm. *Studies in Computational Intelligence*, **798**, 357–368 (2018).

[12] Gálvez, A., Iglesias, A.: Computational intelligence CSA-based approach for machine-driven calculation of outline curves of cutaneous melanoma. Proc. of Int. Conf. on Cyberworlds, CW-2018, Singapore. IEEE CS Press, 270–275 (2018).

[13] Gálvez, A., Fister, I., Osaba, E., Fister Jr., I., Del Ser, J., Iglesias, A.: Hybrid modified firefly algorithm for border detection of skin lesions in medical imaging. Proc. of IEEE Congress on Evolutionary Computation, IEEE CEC 2019, Wellington, New Zealand. IEEE (*in press*).

[14] Gálvez, A., Osaba, E., Del Ser, J., Iglesias, A.: Bat algorithm for kernel computation in fractal image reconstruction. Proc. of Int. Conf. on Comp. Science, ICCS 2019. *Lecture Notes in Computer Science* (*in press*).

[15] Garnavi, R. Aldeen, M., Celebi, M.E., Varigos, G., Finch, S.: Border detection in dermoscopy images using hybrid thresholding on optimized color channels. *Computerized Medical Imaging and Graphics*, **35**(2), 105–115 (2011).

[16] Iglesias, A., Gálvez, A., Collantes, M.: Multilayer embedded bat algorithm for B-spline curve reconstruction. *Integrated Computer-Aided Engineering*, **24**(4), 385–399 (2017).

[17] Iglesias, A., Gálvez, A., Collantes, M.: Iterative sequential bat algorithm for free-form rational Bézier surface reconstruction. *International Journal of Bio-Inspired Computation*, **11**(1), 1–15 (2018).

[18] Kashi, S., Minuchehr, A., Poursalehi, N., Zolfaghari, A.: Bat algorithm for the fuel arrangement optimization of reactor core. *Annals of Nuclear Energy*, **64**, 144–151 (2014).

[19] Kaveh, A.,Zakian, P.: Enhanced bat algorithm for optimal design of skeletal structures. *Asian Journal Civil Engineering*, **15**(2), 179–212 (2014).

[20] Korotkov, K., Garcia, R.: Computerized analysis of pigmented skin lesions: a review. *Artificial Intelligence in Medicine*, **56**, 69–90 (2012).

[21] Latif, A., Palensky, P.: Economic dispatch using modified bat algorithm. *Algorithms*, **7**(3), 328–338 (2014).

[22] Ma, Z., Tavares, J.M.: A novel approach to segment skin lesions in dermoscopic images based on a deformable model. *IEEE Journal of Biomedical and Health Informatics*, **20**, 615–623 (2016).

[23] Machado, D.A., Giraldi, G., Novotny, A.A.: Multi-object segmentation approach based on topological derivative and level set method. *Integrated Computer-Aided Engineering*, **18**, 301–311 (2011).

[24] Nachbar, F., Stolz, W., Merkle, T., Cognetta, A.B., Vogt, T., Landthaler, M., Bilek, P., Braun-Falco, O., Plewig, G.: The ABCD rule of dermatoscopy. High prospective value in the diagnosis of doubtful melanocytic skin lesions. *Journal American Academy of Dermatology*, **30**(4), 551–559 (1994).

[25] Pathan, S., Prabhu, K.G., Siddalingaswamy, P.C.: Techniques and algorithms for computer aided diagnosis of pigmented skin lesions – a review. *Biomedical Signal Processing and Control*, **39**, 237–262 (2018).

[26] Piegl, L., Tiller, W.: *The NURBS Book*, Springer Verlag, Berlin Heidelberg (1997).

[27] Schmid, P.: Segmentation of digitized dermatoscopic images by two-dimensional color clustering. *IEEE Transactions on Medical Imaging*, **18**(2), 164–171 (1999).

[28] Suárez, P., Iglesias, A.: Bat algorithm for coordinated exploration in swarm robotics. *Advances in Intelligent Systems and Computing*, **514**, 134–144 (2017).

[29] Suárez, P., Gálvez, A., Iglesias, A.: Autonomous coordinated navigation of virtual swarm bots in dynamic indoor environments by bat algorithm. Int. Conf. in Swarm Intelligence, ICSI 2017. *Lecture Notes in Computer Science*, **10386**, 176–184 (2017).

[30] Suárez, P., Gálvez, A., Fister, I., Fister Jr., I., Osaba, E., Del Ser, J., Iglesias, A.: Bat algorithm swarm robotics approach for dual non-cooperative search with self-centered mode. Int. Conf. on Intelligent Data Engineering and Automated Learning, IDEAL 2018. *Lecture Notes in Computer Science*, **11315**, 201–209 (2018).

[31] Suárez, P., Iglesias, A., Gálvez, A.: Make robots be bats: specializing robotic swarms to the bat algorithm. *Swarm and Evolutionary Computation*, **44**, 113–129 (2019).

[32] Yang, X.-S.: *Nature-Inspired Metaheuristic Algorithms (2nd. Edition)*. Luniver Press, Frome, UK (2010).

[33] Yang, X.S.: A new metaheuristic bat-inspired algorithm. *Studies in Computational Intelligence*, Springer Berlin, **284**, 65–74 (2010).

[34] Yang, X. S..: Bat algorithm for multiobjective optimization. *Int. J. Bio-Inspired Computation*, **3**(5) (2011), 267-274.

[35] Yang, X.S., Gandomi, A.H.: Bat algorithm: a novel approach for global engineering optimization. *Engineering Computations*, **29**(5) (2012), 464–483.

[36] Yang, X.S.: Bat algorithm: literature review and applications. *Int. J. Bio-Inspired Computation*, **5**(3) (2013), 141–149.

[37] Zhou, H., Schaefer, G., Sadka, A., Celebi, M.E.: Anisotropic mean shift based fuzzy c-means segmentation of dermoscopy images. *IEEE Journal of Selected Topics in Signal Processing*, **3**(1) 26–34 (2009).